Forced vibration analysis of a viscoelastic polymeric piezoelectric microplate with fluid interaction

Amir Monemian Esfahani[1], *Mohsen Bahrami*[1] ✉, *Seyed Reza Ghaffarian Anbarani*[2]

[1]*Department of Mechanical Engineering, Amirkabir University of Technology (Tehran Polytechnic), 1591634311 Tehran, Iran*
[2]*Department of Polymer Engineering, Amirkabir University of Technology (Tehran Polytechnic), Tehran, Iran*
✉ *E-mail: mbahrami@aut.ac.ir*

Published in Micro & Nano Letters; Received on 13th February 2016; Revised on 28th April 2016; Accepted on 29th April 2016

The equations of motion for a viscoelastic polymeric piezoelectric microplate are established based on the thin plate theory and Kelvin–Voigt laws. Polyvinylidene fluoride is chosen as the polymeric piezoelectric material. The plate is assumed to be rectangular and the boundary conditions are clamped at all edges. Liquid is modelled as a damping foundation beneath the plate. The equations are solved using assumed-mode method along with Newmark's β method. The effects of variation in the input voltage, damping coefficient, viscoelastic parameter, and excitation frequency are discussed. The results are compared with the developed finite element method. An excellent agreement is observed between the two methods.

1. Introduction: Applications of biomedical microelectromechanical systems (BioMEMS) are of special interest to researchers, and microfluidic devices are rapidly garnering interest [1]. However, dynamic modelling of these systems is still a challenging issue [2–4]. Understanding the dynamic behaviour of microfluidic devices is therefore essential for better design and control actions.

Polyvinylidene fluoride (PVDF) is a polymer piezoelectric material, which, for actuation applications, is often available as a thin film. Some researchers have investigated the piezoelectric properties of polymers. In 1969, Kawai [5] examined the piezoelectric properties of PVDF. Furukawa [6] explored piezoelectricity in ferroelectric polymers. Fukada [7] made a review on piezoelectric polymers in 2000. Riande and Calleja [8] worked on electrical properties of polymers in 2004. PVDF has been investigated in recent years for application in BioMEMS devices. Polymers such as PVDF have gained popularity over the past few years for their biocompatibility, ease of production, and relatively low cost compared with silicon and ceramic materials [9]. In 2008, Tanaka *et al.* [10] used PVDF films for evaluating tactile sensations. Carpi *et al.* [11] studied biomedical applications of electroactive polymers. Seminara *et al.* investigated the electromechanical properties of PVDF polymer films for application in robotic tactile sensors. They set up an experimental procedure for the measurement of the PVDF characteristics [12]. Chiu *et al.* [13] developed a PVDF sensor patch for heartbeat monitoring. Note that no theoretical modelling had been mentioned in this Letter. Moleiro *et al.* proposed an exact solution for static analysis of multilayered PVDF. Different loading conditions and plate aspect ratios were investigated [14]. Jaitanong *et al.* worked on PVDF composite structures. They studied piezoelectric properties of cement-based/PVDF/PZT [15]. Duan *et al.* [16] used PVDF piezoelectric films as sound absorption material. They also proposed a flexible microperforated panel based on PVDF films for this purpose. Monemian Esfahani and Bahrami [17] performed free vibration analysis of PVDF circular microplate.

To solve the equations describing the behaviour of piezoelectric materials, some numerical methods have been proposed. In 1990, Tzou and Tseng [18] analysed a two-dimensional (2D) piezoelectric material by finite element method (FEM) for use as an actuator or a sensor. Kagawa *et al.* [19] applied FEM for simulating a piezoelectric actuator. Khutoryansky *et al.* [20] used boundary element method to model and simulate active materials. Benjeddou [21] investigated FEM for some structures such as shells and plates. Jun and Zhaowei [22] surveyed FEM to investigate the performance of piezoelectric actuator in hard disk drives.

In this Letter, governing equations are derived using piezoelectric constitutive equations in fully general form. Fluidic media is modelled as a damping foundation acting beneath the plate. The viscoelastic property of PVDF is introduced into the governing equations using Kelvin–Voigt laws. Boundary conditions are assumed to be clamped at all the edges, which is the condition for most microdevices, while it adds more complexity to the problem. The governing equations are solved using assumed-modes method and Newmark's β method. MATLAB codes are generated to solve the equation. A finite element model is then developed using COMSOL multiphysics package to verify the solution. The effect of parameters such as the damping coefficient, viscoelastic parameter, input voltage, and excitation frequency are investigated.

2. Problem formulation: Figure 1 shows the configuration of the microplate. As shown in this figure, length, width, and thickness of the plate are indicated as b, a, and h, respectively. The plate is a monolayer and the input voltage is applied between the upper and lower surfaces of the plate.

The piezoelectric constitutive equations are as follows

$$\varepsilon_p = s^E_{pq}\sigma_q + d_{pi}E_i \tag{1}$$

$$D_i = d_{ip}\sigma_q + \xi^\sigma_{ij}E_i \tag{2}$$

where $\boldsymbol{\varepsilon}$ is the strain vector, $\boldsymbol{\sigma}$ is the stress vector, $\boldsymbol{E}$ is the electric field vector, $\boldsymbol{D}$ is the displacement vector, $\boldsymbol{s}$ is the compliance coefficients matrix, $\boldsymbol{d}$ is the matrix of piezoelectric strain constants, and ξ is the permittivity constants matrix. The indices $i, j = 1, 2, 3$ and p,

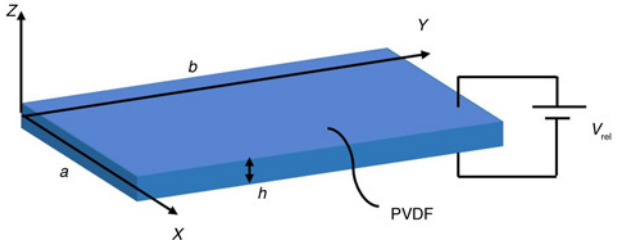

Fig. 1 *Configuration of the microplate*

$q = 1, 2, \ldots, 6$ refer to different directions within the material coordinate system.

Equation (1) is used for actuation and (2) is used for sensing purposes. These equations are rewritten more conveniently as follows

$$\sigma_p = c^E_{pq}\varepsilon_q - h_{pi}D_i \tag{3}$$

$$E_i = -h_{ip}\varepsilon_q + \beta^{\varepsilon}_{ij}D_i \tag{4}$$

$$\sigma_p = c^E_{pq}\varepsilon_q - e_{pi}E_i \tag{5}$$

$$D_i = e_{ip}\varepsilon_q + \xi^{\varepsilon}_{ij}E_i \tag{6}$$

where $c^E_{pq} = \left(\partial\sigma_p/\partial\varepsilon_q\right)_D$ is the elastic stiffness coefficients matrix under constant dielectric displacement, $\boldsymbol{\beta}$ refers to constant or zero strain condition for the impermittivity constants matrix, $h_{pi} = -(1/d_{pi})$ is the matrix of piezoelectric constants, and $e = \xi.h$.

Equations (3) and (4) are used for sensing and (5) and (6) are used for actuation. Considering thin plate theory, (6) for an anisotropic piezoelectric material can be rewritten in matrix form as

$$\begin{Bmatrix} D_x \\ D_y \\ D_z \end{Bmatrix} = \begin{bmatrix} 0 & 0 & 0 & e_{15} & 0 \\ 0 & 0 & 0 & 0 & e_{25} \\ e_{31} & e_{32} & 0 & 0 & 0 \end{bmatrix} \begin{Bmatrix} \varepsilon_{xx} \\ \varepsilon_{yy} \\ \varepsilon_{xy} \\ \varepsilon_{xz} \\ \varepsilon_{yz} \end{Bmatrix} + \begin{bmatrix} \xi_{11} & 0 & 0 \\ 0 & \xi_{22} & 0 \\ 0 & 0 & \xi_{33} \end{bmatrix} \begin{Bmatrix} 0 \\ 0 \\ E_z \end{Bmatrix} \tag{7}$$

The electric displacement components must satisfy the following condition [24]

$$\frac{\partial D_x}{\partial x} + \frac{\partial D_y}{\partial y} + \frac{\partial D_z}{\partial z} = 0 \tag{8}$$

Substituting (7) into (8) and assuming $\boldsymbol{E}_z = \partial V/\partial z$, where V is the applied electric potential, results in

$$e_{15}\frac{\partial \varepsilon_{xz}}{\partial x} + e_{25}\frac{\partial \varepsilon_{yz}}{\partial y} + e_{31}\frac{\partial \varepsilon_{xx}}{\partial z} + e_{32}\frac{\partial \varepsilon_{yy}}{\partial z} - \xi_{33}\frac{\partial^2 V}{\partial z^2} = 0 \tag{9}$$

On the basis of Kirchhoff plate theory, all displacements are related to the transverse displacement

$$\varepsilon_{xx} = -z\frac{\partial^2 w}{\partial x^2} \tag{10}$$

$$\varepsilon_{yy} = -z\frac{\partial^2 w}{\partial y^2} \tag{11}$$

$$\varepsilon_{xy} = -2z\frac{\partial^2 w}{\partial x \partial y} \tag{12}$$

$$\varepsilon_{xz} = \frac{\partial u}{\partial z} + \frac{\partial w}{\partial x} \tag{13}$$

$$\varepsilon_{yz} = \frac{\partial v}{\partial z} + \frac{\partial w}{\partial y} \tag{14}$$

Substituting (10)–(14) into (9) yields the relation between the applied electric potential (V) and the transverse displacement (w) for a piezoelectric plate as follows

$$e_{31}\frac{\partial^2 w}{\partial x^2} + e_{32}\frac{\partial^2 w}{\partial y^2} = \boldsymbol{\xi}_{33}\frac{\partial^2 V}{\partial z^2} \tag{15}$$

If the relative electric potential between the top and bottom of the plate is assumed to be V_{rel}, integrating (15) twice, we have

$$V = \frac{1}{\xi_{33}}\left(e_{31}\frac{\partial^2 w}{\partial x^2} + e_{32}\frac{\partial^2 w}{\partial y^2}\right)\left(\frac{z^2}{2} - \frac{h^2}{8}\right) + V_{\text{rel}}\left(\frac{z}{h} + \frac{1}{2}\right) \tag{16}$$

For a viscoelastic material, which obeys the Kelvin–Voigt laws, Hooke's law is written as follows

$$\boldsymbol{\sigma} = \boldsymbol{E}(\boldsymbol{\varepsilon} + \eta\dot{\boldsymbol{\varepsilon}}) \tag{17}$$

where η is the viscous coefficient. The dot sign indicates differentiation with respect to time.

By expanding Hooke's law for linear material, the total stress (including mechanical and electrical components) in a viscoelastic piezoelectric plate can be written as follows

$$\sigma_{xx} = -\frac{Ez}{(1-\nu^2)}\left(\frac{\partial^2 w}{\partial x^2} + \eta\frac{\partial^3 w}{\partial t \partial x^2}\right) - \frac{Ez\nu}{(1-\nu^2)}\left(\frac{\partial^2 w}{\partial y^2} + \eta\frac{\partial^3 w}{\partial t \partial y^2}\right) + e_{31}\frac{\partial V}{\partial z} \tag{18}$$

$$\sigma_{yy} = -\frac{Ez}{(1-\nu^2)}\left(\frac{\partial^2 w}{\partial y^2} + \eta\frac{\partial^3 w}{\partial t \partial y^2}\right) - \frac{Ez\nu}{(1-\nu^2)}\left(\frac{\partial^2 w}{\partial x^2} + \eta\frac{\partial^3 w}{\partial t \partial x^2}\right) + e_{32}\frac{\partial V}{\partial z} \tag{19}$$

$$\sigma_{xy} = -\frac{Ez}{(1+\nu)}\left(\frac{\partial^2 w}{\partial x \partial y} + \eta\frac{\partial^3 w}{\partial t \partial x \partial y}\right) \tag{20}$$

Using (18)–(20), the resultant bending moments are (see equations (21) and (22))

$$M_{xy} = -\frac{Eh^3(1-\nu)}{12(1-\nu^2)}\left(\frac{\partial^2 w}{\partial x \partial y} + \eta\frac{\partial^3 w}{\partial t \partial x \partial y}\right) \tag{23}$$

The in-plane forces are defined as follows

$$N_x = \int_{-(h/2)}^{h/2} \sigma_{xx}\,\mathrm{d}z = e_{31}V \tag{24}$$

$$N_y = \int_{-(h/2)}^{h/2} \sigma_{yy}\,\mathrm{d}z = e_{32}V \tag{25}$$

The resulting shear forces are then obtained from the following equations

$$Q_x = \frac{\partial M_{xx}}{\partial x} + \frac{\partial M_{xy}}{\partial y} \tag{26}$$

$$Q_y = \frac{\partial M_{yy}}{\partial y} + \frac{\partial M_{xy}}{\partial x} \tag{27}$$

$$M_{xx} = \frac{h^3}{12}\left(-\frac{E}{(1-\nu^2)}\left(\frac{\partial^2 w}{\partial x^2} + \eta\frac{\partial^3 w}{\partial t \partial x^2}\right) - \frac{E\nu}{(1-\nu^2)}\left(\frac{\partial^2 w}{\partial y^2} + \eta\frac{\partial^3 w}{\partial t \partial y^2}\right) + \frac{e_{31}^2}{\xi_{33}}\frac{\partial^2 w}{\partial x^2} + \frac{e_{31}e_{32}}{\xi_{33}}\frac{\partial^2 w}{\partial y^2}\right) \tag{21}$$

$$M_{yy} = \frac{h^3}{12}\left(-\frac{E}{(1-\nu^2)}\left(\frac{\partial^2 w}{\partial y^2} + \eta\frac{\partial^3 w}{\partial t \partial y^2}\right) - \frac{E\nu}{(1-\nu^2)}\left(\frac{\partial^2 w}{\partial x^2} + \eta\frac{\partial^3 w}{\partial t \partial x^2}\right) + \frac{e_{32}^2}{\xi_{33}}\frac{\partial^2 w}{\partial y^2} + \frac{e_{31}e_{32}}{\xi_{33}}\frac{\partial^2 w}{\partial x^2}\right) \tag{22}$$

doi: 10.1049/mnl.2016.0043

The dynamic equilibrium equation in the z-direction for an infinitesimal element of a rectangular plate with fluid interaction is given as

$$\frac{\partial Q_x}{\partial x}+\frac{\partial Q_y}{\partial y}+N_x\frac{\partial^2 w}{\partial x^2}+N_y\frac{\partial^2 w}{\partial y^2}-c\frac{\partial w}{\partial t}=\rho h\frac{\partial^2 w}{\partial t^2} \tag{28}$$

where c is the fluid viscous damping, ρ and h are the plate density and thickness, respectively.

Substituting (24)–(27) into (28), the governing equation is obtained (see (29))

3. Orthogonal polynomials generation for 2D problem: For generating the orthogonal function, Gram–Schmidt method is used [25]. In this method, the first polynomial is assumed to be as follows

$$\varphi_1=F_1=g(x,\ y)f_1 \tag{30}$$

where $g(x,\ y)$ is the function satisfying the essential boundary conditions and the starting function f_1 dictates the frequency generated by the following algorithm:

1. Symmetric–symmetric mode: $f_1=1$.
2. Symmetric–antisymmetric mode: $f_1=X$.
3. Antisymmetric–symmetric mode: $f_1=Y$.
4. Antisymmetric–antisymmetric mode: $f_1=XY$.

The remaining polynomials are then derived as follows

$$\varphi_2=F_2=x^2\varphi_1-\alpha_{21}\varphi_1 \tag{31}$$

$$\varphi_3=F_3=y^2\varphi_1-\alpha_{31}\varphi_1-\alpha_{32}\varphi_2 \tag{32}$$

where

$$\alpha_{21}=\frac{x^2\varphi_1|\ \varphi_1}{\varphi_1|\varphi_1} \tag{33}$$

$$\alpha_{31}=\frac{y^2\varphi_1|\ \varphi_1}{\varphi_1|\varphi_1} \tag{34}$$

$$\alpha_{32}=\frac{y^2\varphi_1|\ \varphi_2}{\varphi_2|\varphi_2} \tag{35}$$

and the operator | is the inner product of the functions and is defined as

$$p|q=\iint_R p(x,\ y)q(x,\ y)\,\mathrm{d}x\,\mathrm{d}y \tag{36}$$

4. Forced vibration of the plate: Assume the spatial function to be as follows

$$w(x,\ y,\ t)=\sum_{i=1}^{N}T_i(t)\varphi_i(x,\ y) \tag{37}$$

Applying (37) into (29) yields (see (38))

Now, both sides of (38) are multiplied by orthogonal mode $\phi\phi_j$ and integrated over the domain R. The following equation is then obtained

$$[\boldsymbol{M}]\{\ddot{T}\}+[\boldsymbol{C}]\{\dot{T}\}+[K]\{T\}=V\ \sin(\omega t)[\boldsymbol{q}]\{T\} \tag{39}$$

where

$$M_{ij}=\iint_R \rho h\varphi_i\varphi_j\,\mathrm{d}x\,\mathrm{d}y \tag{40}$$

(see (41))

(see equation (42) at the bottom of the next page)

$$q_{ij}=\iint_R -\left(e_{31}\frac{\partial}{\partial x}\varphi_i\frac{\partial}{\partial x}\varphi_j+e_{32}\frac{\partial}{\partial y}\varphi_i\frac{\partial}{\partial y}\varphi_j\right) \tag{43}$$

From (39), one can observe that the solution of this equation with zero initial conditions is zero. To solve this problem, we need to apply initial conditions or some pressure on the plate. The latter is chosen here, as it can be assumed that the fluid is acting on the upper surface of the plate. The derived equations will not change as the effect of damping is in the opposite direction of the movement, whether it acts on the upper surface or the lower one.

$$\left(\frac{Eh^3}{12(1-\nu^2)}-\frac{e_{31}^2h^3}{12\xi_{33}}\right)\frac{\partial^4 w}{\partial x^4}+\left(\frac{Eh^3\nu}{6(1-\nu^2)}+\frac{4Eh^3}{(1-\nu^2)}-\frac{4Eh^3\nu}{(1-\nu^2)}-\frac{e_{31}e_{32}h^3}{6\xi_{33}}\right)\frac{\partial^4 w}{\partial^2 x\partial^2 y}+\left(\frac{Eh^3\nu}{6(1-\nu^2)}-\frac{e_{32}^2h^3}{12\xi_{33}}\right)\frac{\partial^4 w}{\partial y^4}+\left(\frac{Eh^3\eta}{12(1-\nu^2)}\right)$$
$$\times\frac{\partial^5 w}{\partial t\partial x^4}+\left(\frac{Eh^3\nu\eta}{6(1-\nu^2)}+\frac{4Eh^3\eta}{(1-\nu^2)}-\frac{4Eh^3\nu\eta}{(1-\nu^2)}\right)\frac{\partial^5 w}{\partial t\partial^2 x\partial^2 y}+\left(\frac{Eh^3\eta}{12(1-\nu^2)}\right)\frac{\partial^5 w}{\partial t\partial y^4}-e_{31}V\frac{\partial^2 w}{\partial x^2}-e_{32}V\frac{\partial^2 w}{\partial y^2}+c\frac{\partial w}{\partial t}+\rho h\frac{\partial^2 w}{\partial t^2}=0 \tag{29}$$

$$\left(\frac{Eh^3}{12(1-\nu^2)}-\frac{e_{31}^2h^3}{12\xi_{33}}\right)\frac{\partial^4}{\partial x^4}\left(\sum_{i=1}^{N}T_i(t)\varphi_i(x,\ y)\right)+\left(\frac{Eh^3\nu}{6(1-\nu^2)}+\frac{4Eh^3}{(1-\nu^2)}-\frac{4Eh^3\nu}{(1-\nu^2)}-\frac{e_{31}e_{32}h^3}{6\xi_{33}}\right)\frac{\partial^4}{\partial^2 x\partial^2 y}\left(\sum_{i=1}^{N}T_i(t)\varphi_i(x,\ y)\right)$$
$$+\left(\frac{Eh^3\nu}{6(1-\nu^2)}-\frac{e_{32}^2h^3}{12\xi_{33}}\right)\frac{\partial^4}{\partial y^4}\left(\sum_{i=1}^{N}T_i(t)\varphi_i(x,\ y)\right)+\left(\frac{Eh^3\eta}{12(1-\nu^2)}\right)\frac{\partial^4}{\partial x^4}\left(\sum_{i=1}^{N}\dot{T}_i(t)\varphi_i(x,\ y)\right)$$
$$+\left(\frac{Eh^3\nu\eta}{6(1-\nu^2)}+\frac{4Eh^3\eta}{(1-\nu^2)}-\frac{4Eh^3\nu\eta}{(1-\nu^2)}\right)\frac{\partial^4}{\partial^2 x\partial^2 y}\left(\sum_{i=1}^{N}\dot{T}_i(t)\varphi_i(x,\ y)\right)+\left(\frac{Eh^3\eta}{12(1-\nu^2)}\right)\frac{\partial^4}{\partial y^4}\left(\sum_{i=1}^{N}\dot{T}_i(t)\varphi_i(x,\ y)\right)$$
$$-e_{31}V\frac{\partial^2}{\partial x^2}\left(\sum_{i=1}^{N}T_i(t)\varphi_i(x,\ y)\right)-e_{32}V\frac{\partial^2}{\partial y^2}\left(\sum_{i=1}^{N}T_i(t)\varphi_i(x,\ y)\right)+c\sum_{i=1}^{N}\dot{T}_i(t)\varphi_i(x,\ y)+\rho h\sum_{i=1}^{N}\ddot{T}_i(t)\varphi_i(x,\ y)=0 \tag{38}$$

$$K_{ij}=\iint_R\left(-\frac{h^3E}{12(1-\nu)^2}\left(\frac{\partial^2}{\partial x^2}\varphi_i\frac{\partial^2}{\partial x^2}\varphi_j+\frac{\partial^2}{\partial y^2}\varphi_i\frac{\partial^2}{\partial y^2}\varphi_j+\nu\left(\frac{\partial^2}{\partial x^2}\varphi_i\frac{\partial^2}{\partial y^2}\varphi_j+\frac{\partial^2}{\partial y^2}\varphi_i\frac{\partial^2}{\partial x^2}\varphi_j\right)\right)-\frac{4Eh^3(1-\nu)}{12(1-\nu)^2}\left(\frac{\partial^2}{\partial x\partial y}\varphi_i\frac{\partial^2}{\partial x\partial y}\varphi_j\right)\right.$$
$$\left.-\frac{h^3}{12}\left(\frac{e_{31}^2}{\xi_{33}}\frac{\partial^2}{\partial x^2}\varphi_i\frac{\partial^2}{\partial x^2}\varphi_j+\frac{e_{31}e_{32}}{\xi_{33}}\frac{\partial^2}{\partial y^2}\varphi_i\frac{\partial^2}{\partial x^2}\varphi_j+\frac{e_{31}e_{32}}{\xi_{33}}\frac{\partial^2}{\partial y^2}\varphi_j\frac{\partial^2}{\partial x^2}\varphi_i+\frac{e_{32}^2}{\xi_{33}}\frac{\partial^2}{\partial y^2}\varphi_i\frac{\partial^2}{\partial y^2}\varphi_j\right)\right)\mathrm{d}x\,\mathrm{d}y \tag{41}$$

Table 1 Parameters

Parameter	Value	Unit
E	1.27×10^{9}	pa
v	0.225	1
ρ	1780	kg/m^3
h	10×10^{-6}	m
a	500×10^{-6}	M
b	500×10^{-6}	m
d_{31}	23×10^{-12}	m/V
d_{32}	$\frac{23 \times 10^{-12}}{5}$	m/V
ξ_{33}	106×10^{-12}	F/m

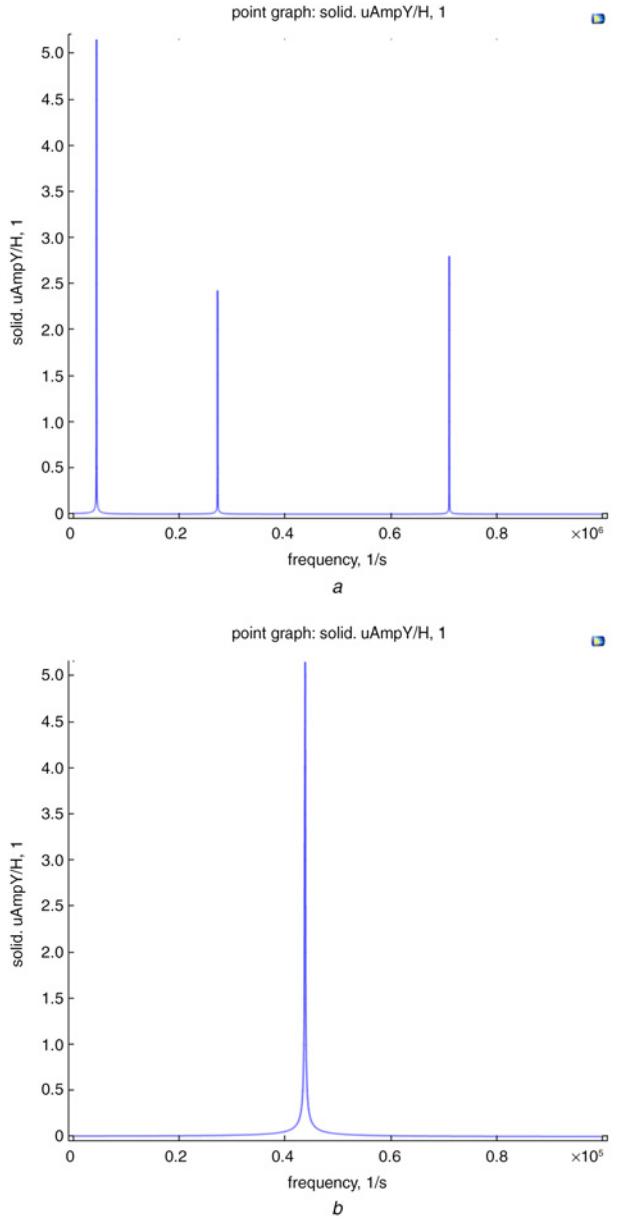

Fig. 2 *Frequency against maximum displacement*
a First three modes
b First mode

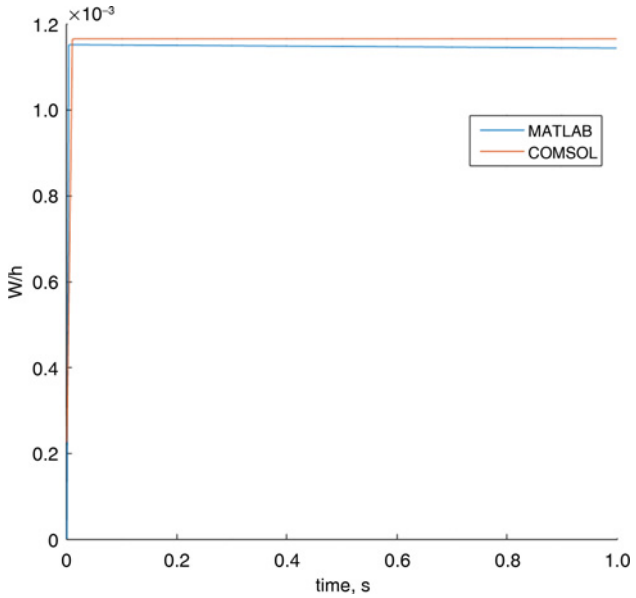

Fig. 3 *Non-dimensional displacement over time for V = 0 V*

By applying pressure in (28), (39) will change into

$$[\boldsymbol{M}]\{\ddot{T}\} + [\boldsymbol{C}]\{\dot{T}\} + [K]\{T\} + \{\boldsymbol{P}\} = V \sin(\omega t)[\boldsymbol{q}]\{T\} \tag{44}$$

where

$$P_i = \iint_R p\varphi_i \, \mathrm{d}x \, \mathrm{d}y \tag{45}$$

Since $\boldsymbol{\phi}_i$s are orthogonal functions, matrix $\boldsymbol{M}$ is diagonal; this implies that solving (44) is easier.

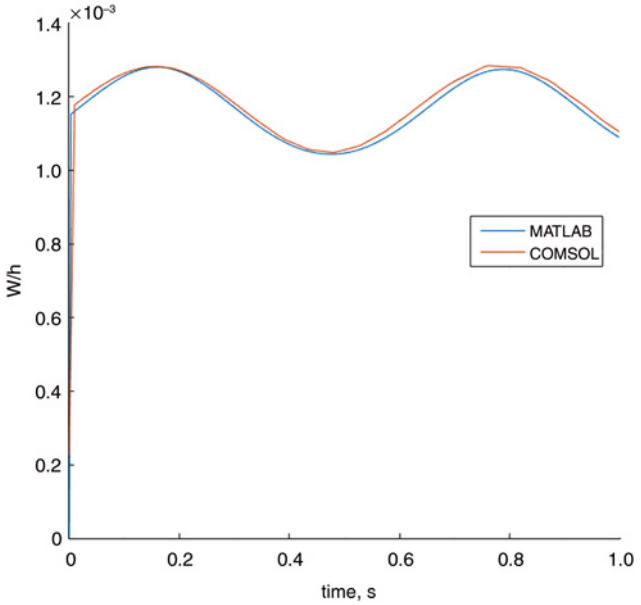

Fig. 4 *Non-dimensional displacement over time for V = 0.15 V*

$$C_{ij} = \iint_R \left(-\frac{h^3 E\eta}{12(1-\nu)^2}\left(\frac{\partial^2}{\partial x^2}\varphi_i \frac{\partial^2}{\partial x^2}\varphi_j + \frac{\partial^2}{\partial y^2}\varphi_i \frac{\partial^2}{\partial y^2}\varphi_j + \nu\left(\frac{\partial^2}{\partial x^2}\varphi_i \frac{\partial^2}{\partial y^2}\varphi_j + \frac{\partial^2}{\partial y^2}\varphi_i \frac{\partial^2}{\partial x^2}\varphi_j\right)\right) - \frac{4Eh^3(1-\nu)\eta}{12(1-\nu)^2}\left(\frac{\partial^2}{\partial x \partial y}\varphi_i \frac{\partial^2}{\partial x \partial y}\varphi_j\right) - c\varphi_i\varphi_j\right) \mathrm{d}x \, \mathrm{d}y \tag{42}$$

doi: 10.1049/mnl.2016.0043

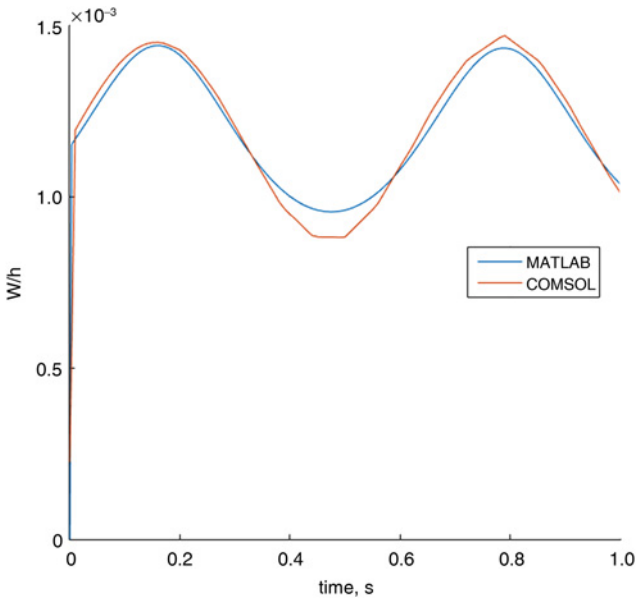

Fig. 5 *Non-dimensional displacement over time for V = 0.37 V*

5. Numerical results: To solve (44), Newmark's β method is used. Newmark [26] proposed a method for solving problems in structural dynamics. This method starts with an initial set of conditions and continues in each time step to obtain the next position, velocity, and acceleration. The relation between consecutive iterations is as follows

$$\ddot{T}_{n+1} = \frac{1}{\beta\Delta t^2}\left(T_{n+1} - T_n\right) - \frac{1}{\beta\Delta t}\dot{T}_n - \left(1 - \frac{1}{2\beta}\right)\ddot{T}_n \quad (46)$$

$$\dot{T}_{n+1} = \frac{\gamma}{\beta\Delta t}\left(T_{n+1} - T_n\right) - \left(\frac{\gamma}{\beta} - 1\right)\dot{T}_n - \left(\frac{\gamma}{2\beta} - 1\right)\Delta t\ddot{T}_n \quad (47)$$

The incremental form of the differential equation is given as follows

$$[\boldsymbol{M}]\{\ddot{T}\}_{n+1} + [\boldsymbol{C}]\{\dot{T}\}_{n+1} + [K]\{T\}_{n+1} + \{\boldsymbol{P}\} = V\ \sin(\omega(n\Delta t))[\boldsymbol{q}]\{T\}_{n+1} \quad (48)$$

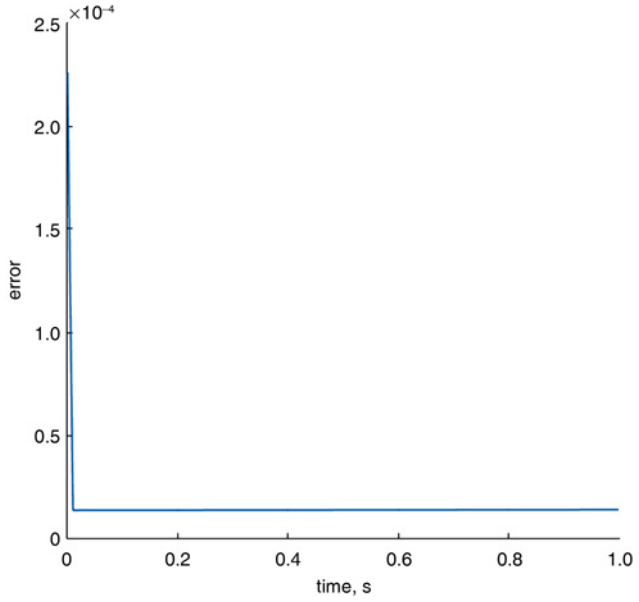

Fig. 6 *Error for V = 0 V*

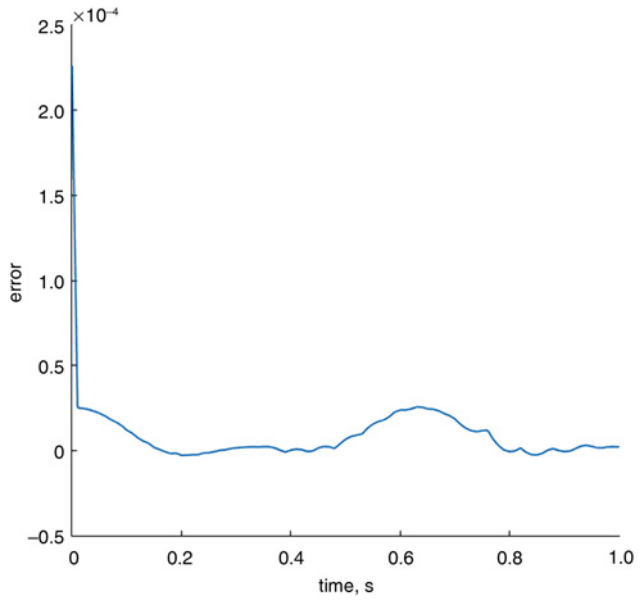

Fig. 7 *Error for V = 0.15 V*

Substituting (46) and (47) into (48) and solving for $\{T\}_{n+1}$, the recurrence relation is obtained.

To obtain the solution, a MATLAB code is written, and the appropriate results are obtained.

The first trial function φ is chosen as follows

$$\varphi_1 = x^2(x-a)^2y^2(y-b)^2 \quad (49)$$

This function is selected in order to satisfy the boundary conditions. Since the boundary conditions are clamped, its value and first derivative must be zero at the edges. The next function is derived using (31).

Table 1 shows the parameters used for numerical simulation.

6. Free vibration analysis of the microplate: To find the natural frequencies of the microplate, free vibration analysis must be applied. For this purpose, the matrices $\boldsymbol{C}$, $\boldsymbol{q}$, and $\boldsymbol{P}$ are assumed to

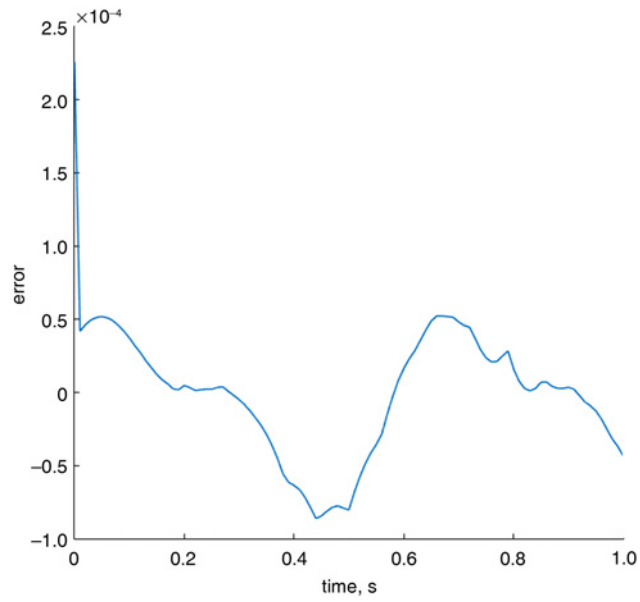

Fig. 8 *Error for V = 0.37 V*

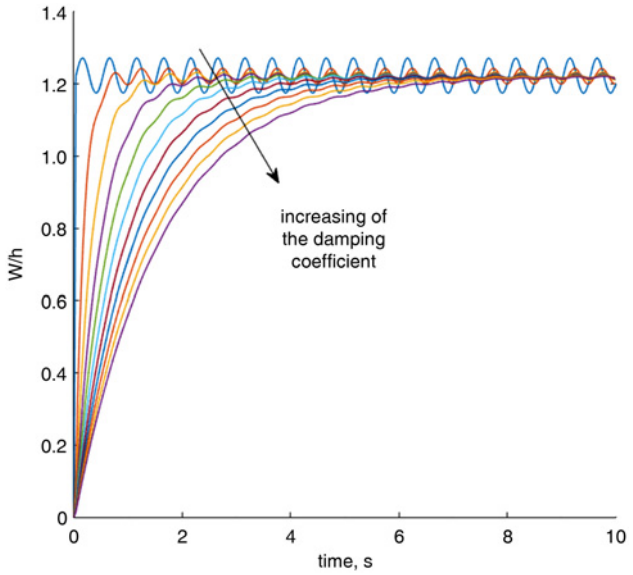

Fig. 9 *Changes in the damping coefficient of the fluid in the absence of the viscoelastic effect*

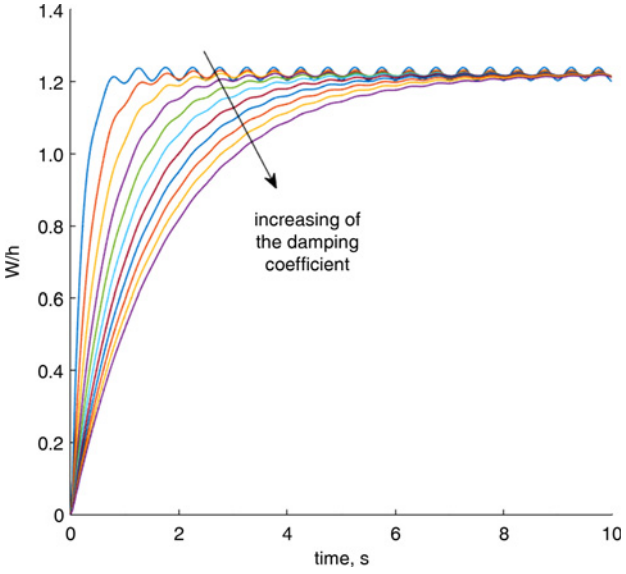

Fig. 11 *Changes in the damping coefficient when the plate is viscoelastic*

be zero matrices. Fig. 2 shows the frequency against maximum displacement.

It can be seen that the first natural frequency occurs at 0.41×10^5 Hz.

7. Finite element model: To verify the results, a finite element model is developed using the COMSOL multiphysics package. A 3D model of the plate is built and imported into the software. The physics of piezoelectric devices and laminar flow were applied to the model. The linear viscoelastic property is added to piezoelectric material.

Figs. 3–5 show the results of both methods.

The results of the two methods have an excellent agreement. The frequencies are equal. The errors are shown in Figs. 6–8. In these figures, the error is defined as the difference between the two methods.

8. Results: Fig. 9 shows the changes in damping coefficient of the fluid in the absence of the viscoelastic effect. By increasing the damping coefficient, the vibration amplitude tends to zero.

Figs. 10 shows the changes in the viscoelastic parameter in the absence of damping effect of the fluid. The behaviour is similar to the one obtained by the change in damping coefficient; the vibration amplitude tends to zero by increasing this parameter.

It can be seen that changes to damping coefficient have more notable effects and the microplate stops damping quickly.

Fig. 11 shows the changes in damping coefficient when the plate is viscoelastic.

Fig. 12 shows the changes in viscoelastic parameter when the plate is interacting with the fluid.

Fig. 13 shows the changes in voltage. As expected, increasing the input voltage causes the amplitude to increase.

Since the upper surface of the plate interacts with fluid, the damping effect is larger; therefore, the amplitude when the plate

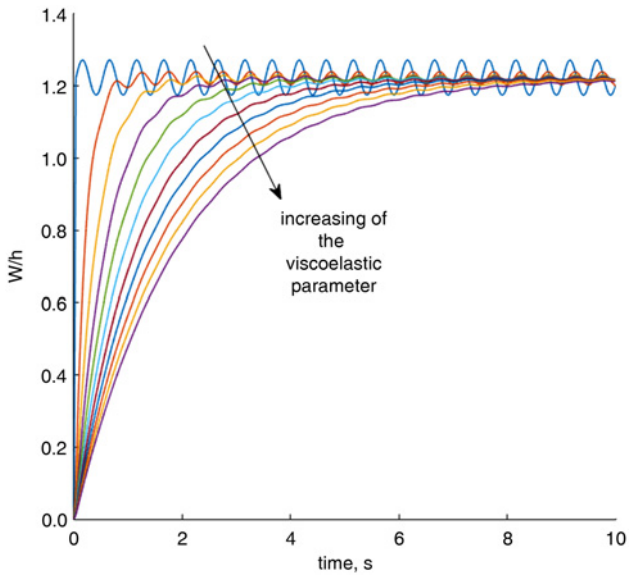

Fig. 10 *Changes in the viscoelastic parameter in the absence of the damping effect of the fluid*

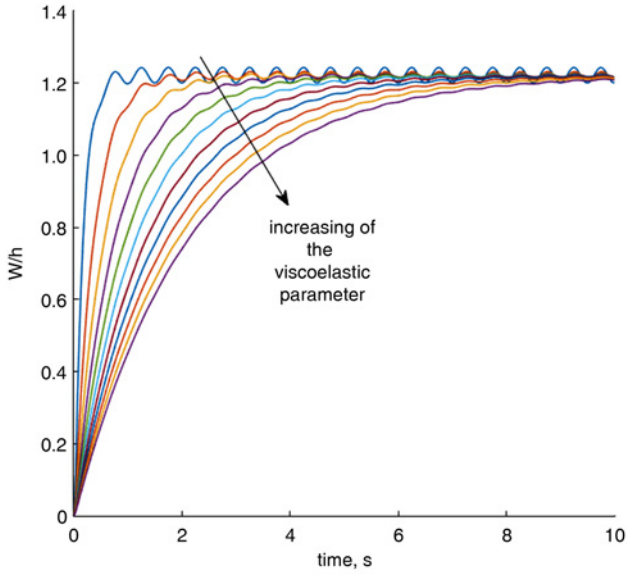

Fig. 12 *Changes in the viscoelastic parameter when the plate is in interaction with fluid*

doi: 10.1049/mnl.2016.0043

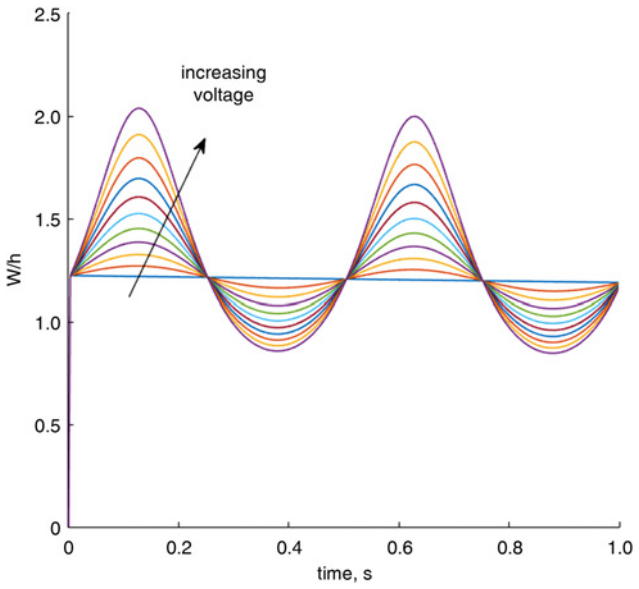

Fig. 13 *Changes in voltage*

moves down is less than when it moves up. Note that all the results are multiplied by -1 to show the results in a suitable form.

9. Conclusion: Forced vibration analysis of a polymeric piezoelectric microplate is presented. The governing equations are derived in the fully general form. For this Letter, PVDF is chosen as the piezoelectric material. Anisotropic piezoelectricity and viscoelastic properties of PVDF are considered. Boundary conditions are assumed clamped at all edges, which are used in many microdevices. Fluid is modelled as a damping foundation applied under the plate. The governing equation is solved using assumed-modes method followed by Newmark's β method. The FEM using COMSOL multiphysics package is applied to the problem. Comparing the results shows an excellent agreement between the two methods, which verifies the equation and the solution. The results show that the effects due to changing the damping coefficient and viscoelastic parameter are the same; however, increasing the damping coefficient of the microplate has a larger effect as the plate will be damped quickly. Increasing the voltage increases the vibration amplitude, but the amplitude in one half of the wave is more than other half because of the damping effect of the fluid.

10. Acknowledgment: This project is supported by the Iran National science foundation (INSF).

11 References

[1] Urban G.A.: 'BioMEMS' (Springer, Dordrecht, The Netherlands, 2006)
[2] Astle A., Bernal L.P., Washabaugh P., *ET AL.*: 'Dynamic modeling and design of a high frequency micro vacuum pump'. ASME 2003, pp. 41–50
[3] Yang R., Zhang M., Tarn T.-J.: 'Dynamic modeling and control of a micro-needle integrated piezoelectric micro-pump for diabetes care'. IEEE-NANO, 2006, pp. 146–149
[4] Hamdan M.N., Abdallah S., Al-Qaisia A.: 'Modeling and study of dynamic performance of a valveless micropump', *J. Sound Vib.*, 2010, **329**, (15), pp. 3121–3136
[5] Kawai H.: 'The piezoelectricity of poly (vinylidene fluoride)', *Jpn. J. Appl. Phys.*, 1969, **10**, pp. 161–171
[6] Furukawa T.: 'Electrostriction and piezoelectricity in ferroelectric polymers', *Jpn. J. Appl. Phys.*, 1984, **23**, pp. L677–L679
[7] Fukada E.: 'History and recent progress in piezoelectric polymers', *IEEE Trans. Ultrason. Ferroelectr. Freq. Control*, 2000, **47**, (6), pp. 1277–1290
[8] Riande E., Calleja R.D.: 'Electrical properties of polymers' (Marcel Dekker, Inc., New York, 2004)
[9] Ferrell N.J., Hansford D.J.: 'Versatile methods for the fabrication of polyvinylidene fluoride microstructures', *Biomed. Microdev.*, 2010, **12**, (6), pp. 1009–1017
[10] Tanaka M., Tanaka Y., Chonan S.: 'Measurement and evaluation of tactile sensations using a PVDF sensor', *J. Intell. Mater. Syst. Struct.*, 2008, **19**, pp. 35–42
[11] Carpi F., Smela E., Harris G.: 'Biomedical applications of electroactive polymer actuators' (Wiley, UK, 2009)
[12] Seminara L., Capurro M., Cirillo P., *ET AL.*: 'Electromechanical characterization of piezoelectric PVDF polymer films for tactile sensors in robotics applications', *Sens. Actuators A*, 2011, **169**, pp. 49–58
[13] Chiu Y.-Y., Lin W.-Y., Wangb H.-Y., *ET AL.*: 'Development of a piezoelectric polyvinylidene fluoride (PVDF) polymer-based sensor patch for simultaneous heartbeat and respiration monitoring', *Sens. Actuators A*, 2013, **189**, pp. 328–334
[14] Moleiro F., Mota Soares C.M., Mota Soares C.A., *ET AL.*: 'Benchmark exact solutions for the static analysis of multilayered piezoelectric composite plates using PVDF', *Compos. Struct.*, 2014, **107**, pp. 389–395
[15] Jaitanong N., Yimnirun R., Zeng H.R., *ET AL.*: 'Piezoelectric properties of cement based/PVDF/PZT composites', *Mater. Lett.*, 2014, **130**, pp. 146–149
[16] Duan X.H., Wang H.Q., Li Z.B., *ET AL.*: 'Sound absorption of a flexible micro-perforated panel absorber based on PVDF piezoelectric film', *Appl. Acoust.*, 2015, **88**, pp. 84–89
[17] Monemian Esfahani A., Bahrami M.: 'Vibration analysis of a circular thin polymeric piezoelectric diaphragm with fluid interaction', *Int. J. Mech. Mater. Des.*, 2015, (1), pp. 1–11, doi: 10.1007/s10999-015-9308-z
[18] Tzou H.S., Tseng C.I.: 'Distributed piezoelectric sensor/actuator design for dynamic measurement/control of distributed parameter system: a piezoelectric finite element approach', *J. Sound Vib.*, 1990, **138**, (1), pp. 17–34
[19] Kagawa Y., Tsuchiya T., Kataoka T.: 'Finite element simulation of dynamic responses of piezoelectric actuators', *J. Sound Vib.*, 1996, **191**, (4), pp. 519–538
[20] Khutoryansky N., Sosa H., Zu W.: 'Approximate greens functions and a boundary element method for electro-elastic analyses of active materials', *Comput. Struct.*, 1998, **66**, pp. 289–299
[21] Benjeddou A.: 'Advances in piezoelectric finite element modeling of adaptive structural elements: a survey', *Comput. Struct.*, 2000, **76**, pp. 347–363
[22] Jun S., Zhaowei Z.: 'Finite element analysis of an IBM suspension integrated with a PZT microactuator', *Sens. Actuators A*, 2002, **100**, pp. 257–263
[23] Jalili N.: 'Piezoelectric-based vibration control from macro to micro/nano scale systems' (Springer Science + Business Media, LLC, Berlin, Germany, 2010)
[24] Ruan X., Danforth S.C., Safari A., *ET AL.*: 'A theoretical study of the coupling effects in piezoelectric ceramics', *Int. J. Solids Struct.*, 1999, **36**, pp. 465–487
[25] Chakraverty S.: 'Vibration of plates' (CRC Press, USA, 2009)
[26] Newmark N.M.: 'A method of computation for structural dynamics', *J. Eng. Mech. Div., ASCE*, 1959, (85), pp. 67–94